American Mineralogist, Volume 92, pages 503–509, 2007

In-situ measurement of dissolution of anorthite in Na-Cl-OH solutions at 22 °C using phase-shift interferometry

Hisao Satoh,[1,*] Yoshihiro Nishimura,[1] Katsuo Tsukamoto,[1] Akira Ueda,[2] Koichi Kato,[2] and Shinzo Ueta[2]

[1]Department of Mineralogy, Petrology and Economic Geology, Tohoku University, Aoba-ku, Sendai 980-8578, Japan
[2]Energy Project and Technology Center, Mitsubishi Materials Corporation Kitabukuro, Omiya, Saitama 330-8508, Japan

Abstract

In-situ measurements of anorthite dissolution in Na-Cl-OH solutions at an ionic strength (IS) of 0.5 mol/L (*M*) and in artificial seawater (IS = 0.7 *M*) were conducted at 22 °C using white-light, phase-shift interference microscopy (PSI-M). Nanometer-scale surface topography by PSI-M revealed three-dimensionally inhomogeneous surface dissolution, which is commonly observed as retreating steps on anorthite surfaces. Continuous dissolution of the anorthite cleavage surface (010) was successfully measured within a day. The vertical dissolution velocity was 4.3×10^{-5} to 1.4×10^{-3} nm/s. The obtained dissolution rates showed a typical dependency on pH with a reaction order of 0.191, and could be consistently extended to the previous data obtained under acidic conditions (Luttge et al. 1999). In-homogeneities in the vertical dissolution velocities at each pH condition could be interpreted by the step dynamics explained by the Burton-Cablera-Frank (BCF) theory (Burton et al. 1951). These results emphasize that the velocity of step retreat is a strong function of the step density, which has to be taken into account when describing the global dissolution phenomena on mineral surfaces.

Keywords: Interferometry, dissolution, anorthite, step dynamics

Introduction

Dissolution of silicates in groundwater recently has been considered an important issue in assessments of the endurance of cement-built underground repositories for supercritical CO_2, for liquid propane gas, and for radioactive wastes. Since late in the last century, dissolution of silicates has been studied extensively by laboratory experiments using wet-chemistry with batch or flow-through methods (Nagy et al. 1992; Burch et al. 1993; Taylor et al. 2000; Cama et al. 2000), which have provided many kinetic data about mineral dissolution rates. Based on these experiments, the rates of mineral dissolution have been interpreted using a rate law that is a function of reactive surface area and that takes into account crystal imperfections (outcrops of dislocations), step density, adsorbed ligands, pH, temperature, pressure, and ΔG of the dissolution reaction (e.g., Lasaga 1995, 1998). Incorporating classical theory for crystal growth, this kinetic model has been recently refined to give the stepwave dissolution model (Lasaga and Luttge 2001), which considers the dissolution not only to be a result of chemical reactions, but also to be a result of step-generation from dislocations and the retreat of the step fronts on the mineral interfaces.

Direct observations of the dissolution of plagioclase surfaces have only been reported by Jordan et al. (1999) for in-situ measurements by atomic force microscopy (AFM) and by Luttge et al. (1999) and Arvidson et al. (2004) for ex-situ measurements by vertical scanning interferometry (VSI). These measurements were performed under acidic conditions (pH-3) or in high-temperature solutions (125–200 °C). Up to now, there was no reported in-situ observation of anorthite dissolution at room temperature and at near-neutral pH, due to the requirement to make long-term measurements to recognize the expected ultra-slow dissolution.

Phase-shift interferometry (PSI) can realize the long-term measurement to quantify dissolution velocities. Laterally, PSI covers a wider scale of interface dissolution (e.g., 100×100 μm) than that of AFM (10×10 μm). Therefore, etch pits or macrosteps in the field of view can be observed more easily. PSI can optically identify topographic features over a vertical scale of less than 1 nm, which is similar to the resolution of AFM. Furthermore, to study realistic reactions at various geo-environmental conditions, PSI allows real-time, in-situ observation at low, as well as elevated, temperature and pressure conditions, if the optical arrangement and the reaction-cell are optimized.

PSI enables quick observation to study transient phenomena. Onuma et al. (1989) established real-time PSI (RPSI) and applied it for the first time to measure the interfacial supersaturation of growing and dissolving K-alum crystals. Using short time-resolution (Δt = 1/60 s), Tsukamoto et al. (1992) applied RPSI for in-situ observation of etch-pit formation on calcite in detail (step velocity = 3–6 nm/s). Nishimura et al. (2004) applied RPSI for ex-situ, 3-dimensional visualization of faint dissolution features on pyrite surfaces (normal velocity = 1E-5 nm/s at pH = 6, by 9 days run). Luttge et al. (1999) applied VSI for the study of anorthite dissolution by ex-situ measurements to quantify the global dissolution volume over the field of view of the interface.

* E-mail: hsatoh@ganko.tohoku.ac.jp

0003-004X/07/0004–503$05.00/DOI: 10.2138/am.2007.2153

Here, we integrated the PSI technique into a microscope (PSI-M), which is optimized to quantify the very slow dissolution of minerals under controlled conditions (temperature, pressure, flow rate, and chemistry). Using PSI-M, we conducted in-situ dissolution measurements of anorthite in aqueous Na-Cl-OH solutions at pH = 7.0–12.4 and a temperature of T = 22 °C. These measurements allow us to interpret the dissolution mechanism attributed to step dynamics.

Optical method

Phase-shift interferometry is 100× more sensitive over the vertical scale than conventional interferometry. Therefore, the topographic survey could be achieved precisely for nanometer-scale dissolution on pyrite (Nishimura et al. 2004). The phase-shift interferogram which differs from the fringes in conventional interferograms, corresponds linearly to a height map, consisting of phases that are displayed as contrasts in the interferogram. Our PSI-M was developed from an Olympus *Fabulous* interferometer, which uses modified Linnik-type (Maki-type) interference optics (Fig. 1a). Since the PSI-M is equipped with a Xe-lamp as a non-coherent white light source, the qualities of both bright-field images and phase-shift interferograms are improved compared to laser-based conventional interferometers with speckles. For the special purpose of ultra-slow (1E-5 nm/s) dissolution measurements, the PSI-M system is reinforced with: (1) a heavy-parts assembly; (2) a windshield with internal air-conditioner; (3) an air-actuated sample stage; and (4) an air-suspended optical table, placed in a clean-room laboratory. Using reaction cells with a static flow-system (Fig. 1b), in-situ dissolution measurements can be achieved with high precision even for long-term measurements.

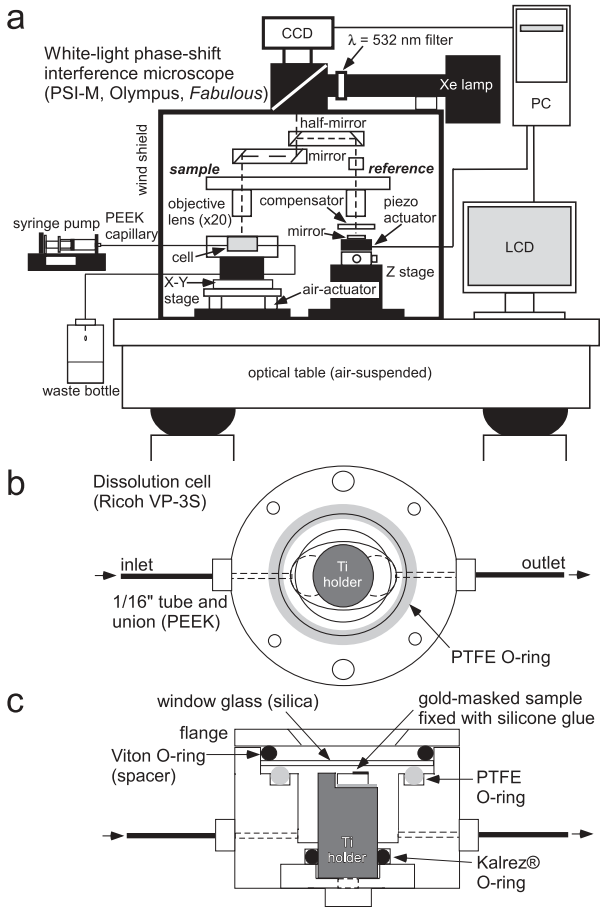

FIGURE 1. A phase-shift interferometry system used for in-situ measurement of dissolution processes showing the optics of the PSI-M and the solution path (**a**), and design of the dissolution cell (**b**: top view; **c**: side view).

Principally, the phase-shift interferogram is obtained from three normal interferograms (fringe interval is 2π) taken at phase positions of 0, 2/3π, and 4/3π by shifting the reference mirror using a piezo actuator (Fig. 1a). Images are captured sequentially by a mega-pixel Peltier cooled CCD camera (Olympus DP70) and PC software (Olympus, DP70 controller) at an acquisition period of >1 s. The collected raw data are in a format of 680 × 512 pixels in 24-bit BMP. Because monochromatic processing at λ = 532 nm was used in this study, the original 24-bit color BMP images are downsized to 8-bit grayscale images (0 to 255 in contrast value). The calculation procedure for a phase-shift interferogram is based on the three conventional interferograms at known phase-shift positions.

The intensity distribution of each fringe can be expressed by the following equation:

$$I_n(x,y) = a(x,y) + b(x,y)\cos[\varphi(x,y) + \delta_n] \quad (1)$$

where I_n is the intensity of the conventional interferogram at each phase-shifting position, a is the background, b is the amplitude of the fringe wavelet, φ is the phase, and δ_n is the phase shift, which is known exactly at position n. When we take I_n at δ_n = 0, 2/3π and 4/3π positions (n = 3), φ as a linearized interferogram can be obtained from each I_n by canceling the other independent variables:

$$\phi(x,y) = \arctan\left(\frac{\sqrt{3}\left[I_3(x,y) - I_2(x,y)\right]}{2I_1(x,y) - I_2(x,y) - I_3(x,y)}\right). \quad (2)$$

The conversion from the contrast of the phase-shift interferogram φ, to the height difference, Δz can be realized on the basis of optical refractive indices of the solutions at 22 °C (n_{22}) as below:

$$\Delta z(x,y) = \frac{\lambda_{532}}{2n_{22}} \times \frac{\Delta I(x,y)}{255} \quad (3)$$

where ΔI is the relative contrast value of the interferogram of the sample to the value of the interferogram of the reference surface:

$$\Delta I(x,y) = I_{\text{sample}}(x,y) - I_{\text{reference}}(x,y). \quad (4)$$

When we use the wavelength of the incident beam monochromized to 532 nm (λ_{532}), the calculated minimum height resolution (Δz) is 0.78 nm for a 0.5 M NaCl solution at 22 °C (n_{22} = 1.338). Normal velocity v_n (m/s) and rate as flux (mol/m²/s) were determined by the following equations,

$$\text{and} \quad v_n(x,y) = \frac{\Delta z(x,y)}{\Delta t} \quad (5)$$

$$rate(x,y) = \frac{v_n(x,y)}{V_M} \quad (6)$$

respectively. Where Δt is the sampling interval and V_M is the molar volume of anorthite (100.75×10^{-6} m^3/mol).

Reference for PSI Measurement

Interferometry is such a sensitive measurement that any disturbance from stage vibration, cell distortion, or variations in ambient conditions (temperature and air draft) cannot be ignored during measurement. To compensate for these disturbances, an insoluble reference is always needed within the observation area. Every interferogram can be normalized to the contrast value of the initial reference surface. This filtering process allows us to obtain an absolute interferogram without disturbance. For ex-situ interferometry, Luttge et al. (1999) utilized a masked pristine mineral surface with silicone glue as an insoluble reference point. However, especially for in-situ measurements, such a mask cannot be used to get an interferogram due to its low reflectance. Furthermore, under a high-pH condition, such glue may suffer alteration and might affect the solution composition.

For ex-situ AFM dissolution measurement on anorthite, Sorai et al. (2002) utilized gold masks made from a sputtered Au coating. In the early trial of our experiments, we also used gold masking prepared by a vacuum-coating method. However, such a coating was easily penetrated by the solution and was not stable over long periods. As a simple method to overcome this problem, we found that the gold nanosheet method is useful for keeping the reference stable (Fig. 1c) and can cancel any disturbance by stage drift and distortion of the cell itself.

Experimental methods

Dissolution runs were carried out using a titanium cell (Fig. 1c) connected to a syringe pump with a 1/16" PEEK capillary. A constant volume flow rate of 47 μL/min was applied. Assuming a fluid depth of 1.0 mm at the crystal holder in the center of the cell, the linear flow velocity over the specimen was estimated to be ~100 μm/s. The experimental temperatures for all the runs were kept at room temperature (i.e., T = 22 ± 0.2 °C, controlled by air-conditioners). Dissolution specimens of anorthite were prepared from cleaved megacrysts of Miyakejima anorthite [Ca/(Ca + Na + K) = 0.96, Jordan et al. 1999]. Anorthite with a gold nanosheet (a few millimeters in size, ~60 nm in thickness) was fixed on a Ti holder with silicone glue (Fig. 1c). The procedures for the preparation of a gold nanosheet reference sample were as follows: (1) a glass side was vacuum coated; (2) the coating was removed by immersion in 1.0 *M* NaOH for several days; (3) the resulting nanosheets were transferred into pure water; and (4) a gold nanosheet was placed manually on each specimen while the sheet was floating in pure water, and was then flattened and fixed by using a heat gun. We tested the gold nanosheets on a substrate of titanium using vertical electron spectroscopy for chemical analysis (ESCA) with Ar-sputtering. Neither Na^+ nor OH^- was significantly detected as residual ions across the coated area. Based on this normalization at an appropriate position on the gold nanosheet ($\Delta I = I_{ano} - I_{gold}$), we can precisely detect the net retreat of the anorthite surface itself, even if disturbances accidentally occurred during long-term measurements. When dissolution takes place at an ultra-slow velocity (~1 μm/year), a long-term measurement that exceeds the statistical error is required to detect the net retreat. This gold nanosheet method can support the PSI-M measurement with sufficient precision.

Solutions were prepared by mixing of 0.5 *M* (mol/L) of NaCl with NaOH to adjust the pH and to maintain a constant ionic strength (IS) of 0.5 *M*. In addition, to represent groundwater of seawater-origin, simulated seawater without carbonate (ASW, 0.469 NaCl + 0.028 $MgCl_2$ + 0.025 $MgSO_4$ + 0.010 $CaCl_2$ mol/L, initial pH = 9.0.) was used for the dissolution run. The optical refractive indices of 0.5 *M* NaCl, 0.5 *M* NaOH solutions, and ASW, and their temperature dependencies, were measured with an Abbe refractometer (Shimadzu Co.) at 20–40 °C. At 22 °C, the optical indices for these NaCl and NaOH solutions were calculated to be 1.3381 ± 0.0006 (SE of linear regression), 1.3380 ± 0.0026, and 1.3430 ± 0.0006, respectively (Table 1). The values of the optical refractive indices for the experimental solutions were calculated on the basis of an ideal mixing assumption.

Dissolution runs were continued up to ~17 h with interferogram acquisitions at every ~1 min. The obtained interferograms were batch-processed by a position-time (x-t) scanning program (TimeLine.exe, E. Yokoyama, pers. comm.) to obtain the normal retreat velocities at the specimen surface.

Results

Because the dissolution of anorthite at pH = 7 and T = 22 °C is expected to be extremely slow, a cleavage step that contains many elementary steps was used as a dissolution surface. Comparing the initial and the final interferograms in an area of 12.6 × 12.6 μm, a very small amount of dissolution was detected successfully. In the 3D topography shown by the initial interferogram, a relatively thick and flat cleavage step can be seen on the pristine (010) surface (Figs. 2a and 2b). However, the final image (t = 67864 s) shows that the surface was slightly eroded and that the step edge had retreated laterally (Figs. 2c and 2d). The height profiles across the step edge before and after the run also exhibit quantitative for evidence dissolution. Against the initial bottom plane (dashed lines in Figs. 2c and 2d), the height differences for the initial and final cleavage-

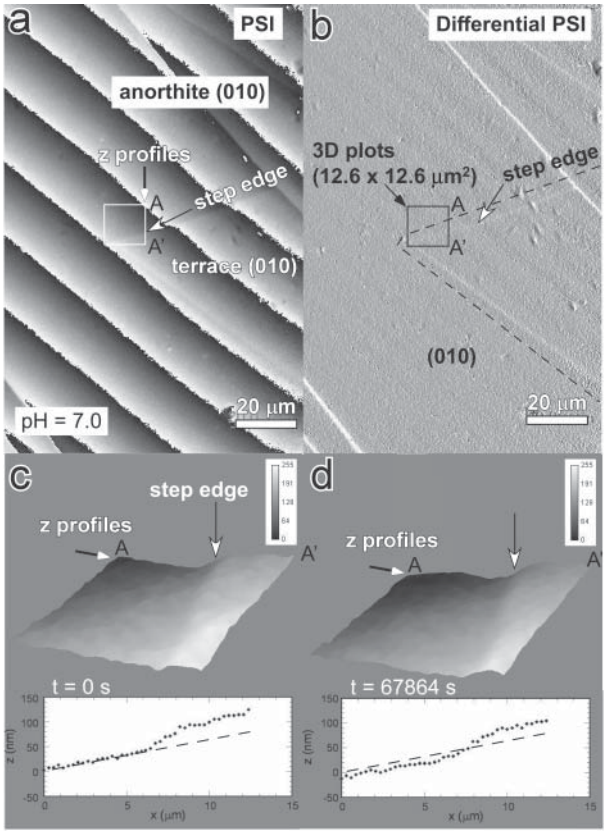

Figure 2. Observed phase-shift interferogram of anorthite (010) in Na-Cl-OH 0.5 *M* solution (pH = 7.0): (**a**) original PSI interferogram showing a slight height contrast at a cleavage step on the (010) face; (**b**) differential interferogram of PSI interferogram (**a**) (= $dI_{x,y}/d_{x-y}$, x-y deferential) visually emphasizing the macrostep occurrence; (**c**) 3-dimensional map of the framed area (12.6 × 12.6 μm) with height profile along the line A-A' before dissolution (t = 0 s), showing flat terraces across a step edge; (**d**) 3-D map with height profile after dissolution (t = 67,864 s), displaying a little retreat both vertically at the terrace and laterally at the edge, in the profile along the line A-A'. Contrast scale (0–255) in the interferograms corresponds to 198.80 nm.

TABLE 1. Experimental conditions for anorthite dissolution

Run no.	Solution	*T* (°C)	pH	IS (M)	flow rate (µL/min)	flow velocity (µm/s)†	refractive index $n_{D,22}$‡	sampling rate (s)
ano-na-ii-70	NaCl	22	7.0	0.5	40	105	1.338	68
ano-na-ii-109	NaCl	22	10.9	0.5	40	105	1.338	66
ano-na-ii-124	NaCl	22	12.4	0.5	40	105	1.338	66
ano-asw-90	ASW*	22	9.0	~0.7	40	105	1.343	66

* Artificial seawater.
† Calculated velocity based on a depth of 1.0 mm at the center of the cell.
‡ Estimated errors are ±0.00059 to ±0.00256 from the standard error of the fitting for *T* vs. n_D plots.

steps display 10 to 25 nm of normal retreat in cross-sections (15 µm in width). This feature further suggests that the dissolution did not occur homogeneously. The most significant retreat was recognized near the slope of the macro-step edge.

The measurements at pH = 12.4 also showed evidence of dissolution. On a cleaved (010) surface with a large number of macrosteps, dissolution occurred successively. This case also showed inhomogeneous dissolution without any proportional retreat of the initial surface over the field of view. The normal dissolution rate near a macro-step edge with a large gap (~70 nm) seems to be enhanced. Thus, local variations were always recognized by in-situ observations of anorthite dissolution under the studied pH conditions, even on a terraced surface without etch pits.

To determine the dissolution rates, we have employed image processing for every set of sequential interferograms by means of: (1) reference-based normalization using the gold nanosheet; and (2) position-time scanning (*x-t* imaging) to accumulate a record of each set of interferograms along a selected line, like a chart records. Using the *x-t* images, height changes at any position along the line can be detected and corresponding velocities can be calculated. Figure 3a shows examples of vertical retreat velocities (nm/s) of anorthite (010) in a 0.5 *M* NaCl solution (pH = 7.0). Two positions at 2.65 and 5.88 µm in the cross-section (Figs. 2c and 2d) were found to exhibit minimum and maximum velocities in the vertical retreat, ranging from $1.96 \pm 0.06 \times 10^{-4}$ to $2.69 \pm 0.08 \times 10^{-4}$ nm/s, respectively (Fig. 3a). The measured positions over the whole surface in the field of view showed a wider velocity range, from $0.43 \pm 0.04 \times 10^{-4}$ to $2.87 \pm 0.09 \times 10^{-4}$ nm/s, than the area profiled in Figure 2. All the observed velocities and their calculated rates are summarized in Table 2.

The positions where the dissolution occurred at various velocities can be identified clearly in the velocity profile across the macrostep edge (Fig. 3b). During the dissolution, height changes at each position mostly showed constant slopes, which suggests that the rate-determining process is related to the step or kink density at the dissolution interface, and it can be assumed that this density is at a steady state during the dissolution processes.

Variations in the observed normal velocity could result from the surface topography and step dynamics. This will be discussed carefully in a later section of this paper. Representative normal retreat rates of the observed surfaces at each pH were tentatively obtained from analyses of random multiple points. It was assumed that the points cover the overall topographic surfaces sufficiently to represent the averaged step density.

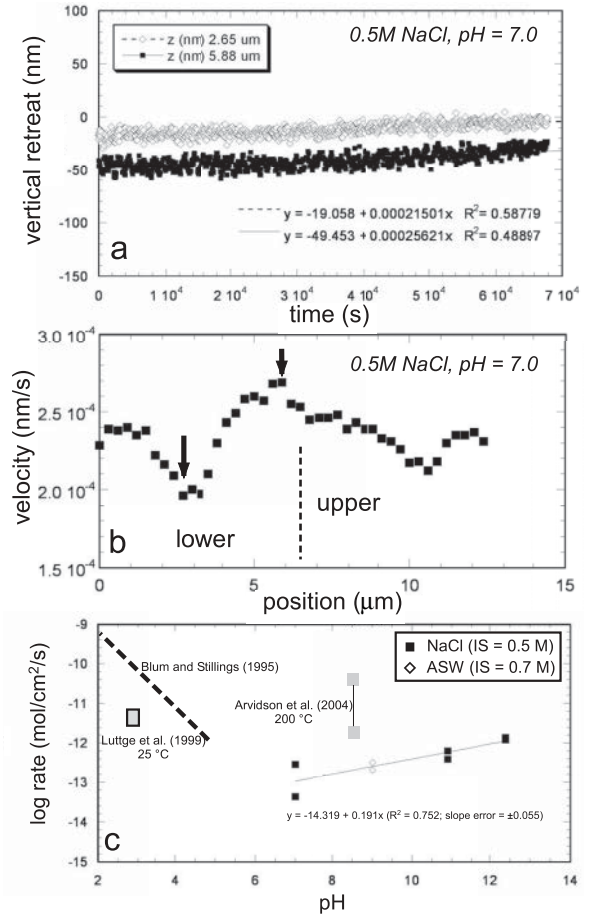

FIGURE 3. (**a**) Examples of in-situ measurements at the positions of x = 2.65 and 5.88 µm on the profile in Figure 2c. These two positions showed the slowest and the fastest velocities (arrows) at this condition (pH = 7.0). (**b**) Distribution of dissolution velocities along the line A-A' shown in Figure 2c. (**c**) Comparison between the normal dissolution rate of anorthite obtained with the PSI method (this study), conventional methods (acidic field: Blum and Stillings 1995), and ex-situ interferometry (VSI: vertical scanning interferometry, Luttge et al. 1999; Arvidson et al. 2004).

DISCUSSION

Rate law

As proposed by Lasaga (1995, 1998), the dissolution rate law can be expressed as in Equation 7:

$$rate = \mathrm{k}_0 \cdot \mathrm{A} \cdot e^{-\mathrm{E}_a / RT} \cdot a_{\mathrm{H}+}{}^{n_{\mathrm{H}+}} \cdot \Pi a_i{}^{n_i} \cdot g(I) \cdot \left\{1 - \exp\left[m \cdot \left(\frac{\Delta G}{RT}\right)^n\right]\right\} \quad (7)$$

In this equation, the rate constant is k_0; the reactive surface area is A; the apparent activation energy is E_a; activities of protons and other ions are represented by a_{H+} and a_i, respectively; and the reaction orders of these ions are represented by n_{H+} and n_i, respectively. The rate is a function of ionic strength $g(I)$, and

undersaturation ΔG [= $RTln(Q/K_{sp})$], where R is the gas-constant, Q is the ionic activity product, and K_{sp} is the solubility product, with log K_{sp} = –20.567 at 22 °C (Arnorsson and Stefansson 1999). The terms m and n are factors depending on the reaction mechanisms (e.g., Cama et al. 2000; m, n = 1 for classical transition state theory).

Lasaga and Luttge (2001) have recently proposed a nonlinear rate law based on the stepwave model. Since the ionic strength and the cationic composition of the solution system are constant for each run, the undersaturation ΔG can also be assumed to be constant for each run. It can be assumed that there will be insignificant changes in the concentrations of components derived from the anorthite at large negative saturation indices, since these occur when the flow rate is very fast (ideally close to $-\infty$ when the flow rate is very fast).

If the dissolution surface is associated with the generation of etch pits, the variable A should be increased. If the dissolution occurs at higher temperature, the rate constant should be increased as a function of $k_0 e^{-Ea/RT}$. In our experiment, no etch pits were recognized in the observed field of view at room temperature (22 °C). Therefore, dissolution should have occurred at a rate near the dissolution plateau for that temperature. Since the cationic concentration of the solution can affect the adsorption of protons on the dissolving surface (Stillings and Brantley 1995; Stillings et al. 1995), we compared the rates at a constant Na^+ concentration while keeping the ionic strength constant. In our experiments, therefore, the logarithms of the rates can be evaluated simply with respect to pH (= –log a_{H+}) and the reaction order. According to Blum and Stillings (1995), the dissolution rate of plagioclase can be expressed as a function of pH and plagioclase composition [e.g., Ca/(Ca + Na + K)], at least under acidic conditions. However, there is no previous report of dissolution rates having been investigated at higher ionic strengths and pH conditions.

pH dependency

We compared the normalized dissolution rates observed by PSI-M (Table 2) with previous data measured under acidic conditions (Blum and Stillings 1995). As shown in the pH vs. log rate plot (Fig. 3c), the dissolution rates increased with increasing pH. Although dissolution in artificial seawater (ASW) was under slightly different conditions with respect to ionic strength (IS ≈ 0.7 M) and a_i, the pH dependency agrees with the trend of the results of the Na-Cl-OH solutions. For the system Na-Cl-OH, anorthite dissolution rate can be expressed as:

$$\log \text{rate} = -14.484 + 0.191\text{pH} \quad (\text{at pH } 7.0\text{–}12.4,\ R^2 = 0.752) \quad (8)$$

showing a small reaction order of pH of 0.191. Previous data obtained by Blum and Stillings (1995) under acidic conditions showed a larger reaction order, and a considerably higher dissolution rate than data obtained from the VSI measurement by Luttge et al. (1999). All the previous data may be consistently extrapolated to a minimum at pH = 7. The VSI data seems to be connected symmetrically to our data, although a significant discrepancy is obvious between data obtained by the powder dissolution method and in-situ measurements. Probably, the powder method tends to show accelerated rates due to enhanced grain boundary dissolution (Arvidson et al. 2003). Our observed small reaction order suggests that the dissolution under basic conditions is not promoted by hydroxyl to as great an extent as under acidic conditions, which is similar to the case of calcite.

Dissolution mechanisms based on step dynamics

Generally, inhomogeneous dissolution is common in most minerals at acidic to neutral conditions. Etch pits are always developed at dissolution centers in the cases of calcite (Tsukamoto et al. 1992; Shiraki et al. 2000) and plagioclase (Luttge et al. 1999, at pH 3 and 25 °C; Jordan et al. 1999, at pH 2 and 125 °C; Arvidson et al. 2004, at pH 8.6 and 200 °C). In basic solutions at 22 °C, no generation of typical etch pits was recognized by in-situ interferometry, but an etched relief appeared in the form of linear steps across the anorthite cleavage surface (Fig. 3b).

The dissolution, which occurred on the interface, substantially consisted of the retreat of elementary steps. Recently, most observations on step behaviors were achieved with AFM (e.g., Pina et al. 1998; Jordan et al. 1999; Davis et al. 2000; Freij et al. 2004). However, AFM can usually monitor only limited areas where step density is moderate, so that it is rather difficult to observe an interface having dense steps and a steep slope. For example, cleavage steps have relatively steep slopes with height differences that might reach ~50 nm over a distance of ~2 μm (Fig. 2). The slope angle relative to the (010) terrace varies from 0 to 2.1°. Based on the measured angle (θ) of the slope, and the measured vertical velocity (v) of the (010) plane, the step velocity of the analyzed slope can be calculated simply by:

$$v_{\text{step}} = \frac{v}{\tan\theta}. \quad (9)$$

The upper limit of slope resolution can be calculated to be 38.7° from the minimum pixel size (~300 nm) and the maximum height contrast for one phase as 2π (~200 nm). The theoretical limit of the slope resolution from PSI can be assumed to be smaller than the pixel-by-pixel slope and is given by a minimum PSI contrast (= 0.78 nm), i.e., 0.15° when the slope is composed of many neighboring steps with the same height and a gap with minimum PSI contrast. If the observed slope is constructed from elementary steps giving a height difference of 1.287 nm (= b) between neighboring pixels (294 nm), the slope can be converted into the number of elementary layers. Using the height of elementary layers (d) and the slope (= tanθ), the interstep distance, λ (nm) can be calculated by:

$$\lambda = \frac{d}{\tan\theta}. \quad (10)$$

These data, v_{step} and λ, can be used to examine the behavior of steps during dissolution. If the crystal growth and dissolution occur at steady-states, so that the surface topography does not change significantly, step dynamics can be interpreted by the BCF theory (Burton et al. 1951), in which the step velocity can be expressed as:

$$v_{\text{step}} = v_\infty \tanh\left(\frac{\lambda}{2X_s}\right), \quad (11)$$

where v_∞ is the maximum velocity for an individual step without any influence from the neighboring steps, and X_s is the surface diffusion distance of solutes liberated from the dissolving step

edge. As shown in Figure 2, the analyzed cleavage step appears as a linear step-front. The dissolution velocity over the analyzed area was constant (Fig. 3a), which suggests that the dissolution process had a steady state.

As shown in Figure 3b, there is a significant variation in normal retreat velocity over the interface across a cleavage macro-step. Such a variation may be explained by the BCF step dynamics. The rate determination for the total surface (e.g., Luttge et al. 1999) may be the average of the varied local rates caused by heterogeneities in step density. However, observation of dissolution as a retreat of isolated steps (v_{step} to v_∞) can provide fundamental information to estimate the overall dissolution of an interface with varied topography.

In Figure 4, two representative examples of the relationship between the calculated λ and the step velocity for the runs at pH = 7.0 and 12.4 are illustrated. Eliminating data with significant error, attributed to the v_{step} estimation at small slopes, these dissolution examples exhibit curves that are well-fitted by the BCF model. Step velocities at pH = 7.0 and 12.4 are estimated to be v_∞ = 0.069 and 0.143 nm/s, respectively, and surface diffusion distances to be X_s = 180 and 168 nm, respectively. Although the estimation may have a large error due to the lack of data, especially at higher λ (i.e., at low angle), it indicates clearly that the step velocity is directly accelerated by pH (i.e., OH^-). On the other hand, if the surface diffusion distance exceeds the interstep width, steep slopes result in a decrease in step velocity by step interaction. Interstep distances typically range from about 0 to several hundreds of nanometers, as observed for the growth of NaCl (Bethge et al. 1968), garnet (Tsukamoto and van der Hoek 1982), and calcite (Davis et al. 2000). For the above cases, the surface diffusion distance (X_s) decreased with an increase in supersaturation (Bethge et al. 1968; Davis et al. 2000). In the case of anorthite dissolution, X_s does not decrease significantly with increase in OH^- (Fig. 4). The variation in X_s can be interpreted to mean that the mean free path of surface-diffusing species such as $Si(OH)_4$ and $Al(OH)_4^-$, given by $X_s = (D_s \Delta t)^{0.5}$ (where D_s is the surface diffusion coefficient as a function of absolute temperature and Δt is the residence time on the terrace), can be decreased by shortening Δt, assuming a constant D_s. Probably, Δt may vary owing to competition between high concentrations of adsorbed OH^- and hydrated species on the interstep terrace.

Thus, room-temperature dissolution of the anorthite (010) surface under basic pH conditions could be explained by the BCF theory (Burton et al. 1951). For mineral dissolution, the retreat velocities of isolated steps that are far from neighboring steps (v_∞) is the most important term, and is corresponds directly to the surface undersaturation. The diffusion distance (X_s) in the presence of competitive molecules is also important for determining the step density and the surface topography. Our advanced PSI-M enabled us to recognize, visualize, and measure the very slow dissolution even at room temperature and neutral pH. Investigation with PSI-M is very useful to survey the dissolution topography (etch pits and steps) and to analyze the dissolution mechanisms attributed to the step dynamics.

This study is the first attempt to recognize, within one day, the very slow dissolution that occurs on insoluble minerals at room temperature. Also, it is an important first achievement for the accurate assessment and validation of mineral dissolution rates around an underground repository for radioactive waste, as well as for natural weathering processes. The next phase of this research program will involve measurement of the dissolution rates of the smectite clay that comprises the engineered barrier of a radioactive waste repository.

TABLE 2. Summary of rate measurements for anorthite dissolution

Run no.	pH	Min/max velocity (nm/s)	Velocity error (±nm/s)*	Rate (mol/cm²/s)†	Log rate (mol/cm²/s)
ano-na-ii-70	7.0	4.32E-05	4.49E-06	4.28E-14	−13.37
	7.0	2.87E-04	8.55E-06	2.85E-13	−12.55
ano-na-ii-109	10.9	3.96E-04	7.14E-05	3.93E-13	−12.41
	10.9	6.40E-04	8.54E-05	6.36E-13	−12.20
ano-na-ii-124	12.4	1.21E-03	3.48E-05	1.20E-12	−11.92
	12.4	1.35E-03	2.75E-05	1.34E-12	−11.87
ano-asw-90	9.0	2.18E-04	8.63E-06	2.16E-13	−12.67
	9.0	3.30E-04	9.13E-06	3.27E-13	−12.48

* Evaluated by the standard error of linear regression.
† Rate conversion based on molar volume as 100.75E-6 m³/mol.

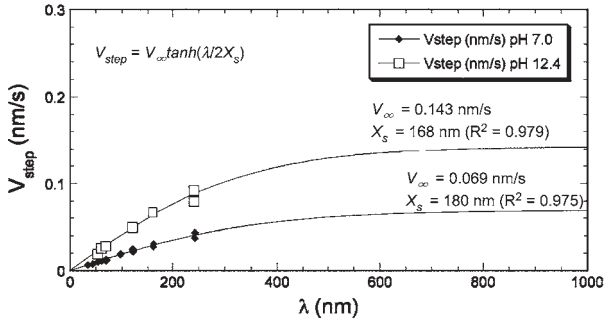

FIGURE 4. Plot of interstep distance, λ vs. step velocity, v_{step}. The fitting curves are based on the BCF theory that estimates both the isolated step velocity (v_∞) and the diffusion distance (X_s) each for the dissolution experiments at pH = 7.0 and 12.4.

ACKNOWLEDGMENTS

We gratefully acknowledge technical support from T. Maki of Olympus Co., for designing the PSI-M optics, and Y. Onuma of Ricoh Co., for setting-up the dissolution cell system. We are also grateful to Y. Furukawa of the Institute of Low-Temperature Sciences, Hokkaido University for assistance in measuring the optical refractive indices of solutions, and to E. Yokoyama of Gakushuin University for computational support to process the interferogram. Discussion with P. Dold of Tohoku University was helpful to improve the manuscript. This study includes results from the research project "Innovative and Viable Nuclear Energy Technology (IVNET) Development Project" funded by the Ministry of Economy, Trade and Industry (METI), Japan.

REFERENCES CITED

Arnorsson, S. and Stefansson, A. (1999) Assessment of feldspar solubility constants in water in the range of 0 degrees to 350 degrees C at vapor saturation pressures. American Journal of Science, 299, 173–209.

Arvidson, R.S., Ertan, I.E., Amonette, J.E., and Luttge, A. (2003) Variation in calcite dissolution rates: A fundamental problem? Geochimica et Cosmochimica Acta, 67, 1623–1634.

Arvidson, R.S., Beig, M.S., and Luttge, A. (2004) Single-crystal plagioclase feldspar dissolution rates measured by vertical scanning interferometry. American Mineralogist, 89, 51–56.

Bethge, H., Keller, K.W., and Ziegler, E. (1968) Molecular processes during crystal growth from the vapor phase. Journal of Crystal Growth, 3–4, 184–187.

Blum, A.E. and Stillings, L.L. (1995) Feldspar dissolution kinetics. In A.F. White and S.L. Brantley, Eds., Chemical Weathering Rates of Silicate Minerals, 31, p. 291–351. Reviews in Mineralogy, Mineralogical Society of America, Chantilly, Virginia.

Burch, T.E., Nagy, K.L., and Lasaga, A.C. (1993) Free energy dependence of albite dissolution kinetics at 80 °C and pH 8.8. Chemical Geology, 105, 137–162.

Burton, W.K., Cabrera, N., and Frank, F.C. (1951) The growth of crystals and the

equilibrium structure of their surfaces. Philosophical Transactions of the Royal Society of London, Series A, 243, 299–358.
Cama, J., Ganor, J., Ayora, C., and Lasaga, A.C. (2000) Smectite dissolution kinetics at 80 °C and pH 8.8. Geochimica et Cosmochimica Acta, 64, 2701–2717.
Davis, K.J., Dove, P.M., and De Yoreo, J.J. (2000) The role of Mg^{2+} as an impurity in calcite growth. Science, 290, 1134–1137.
Freij, S.J., Putnis, A., and Astilleros, J.M. (2004) Nanoscale observations of the effect of cobalt on calcite growth and dissolution. Journal of Crystal Growth, 267, 288–300.
Jordan, G., Higgins, S.R., Eggleston, C.M., Swap, S.M., Janney, D.E., and Knauss, K.G. (1999) Acidic dissolution of plagioclase: In-situ observations by hydrothermal atomic force microscopy. Geochimica et Cosmochimica Acta, 63, 3183–3191.
Lasaga, A.C. (1995) Fundamental approaches in describing mineral dissolution and precipitation rate. In A.F. White and S.L. Brantley, Eds., Chemical Weathering Rates of Silicate Minerals, 31, p. 23–86. Reviews in Mineralogy, Mineralogical Society of America, Chantilly, Virginia.
——— (1998) Kinetic Theory in the Earth Sciences. Princeton University Press, New Jersey.
Lasaga, A.C. and Luttge, A. (2001) Variation of crystal dissolution rate based on a dissolution stepwave model. Science, 291, 2400–2404.
Luttge, A., Bolton, E.W., and Lasaga, A.C. (1999) An interferometric study of the dissolution kinetics of anorthite: the role of reactive surface area. American Journal of Science, 299, 652–678.
Nishimura, Y., Tsukamoto, K., Ueda, A., and Ueta, S. (2004) Development of real-time phase-shift interferometry for extremely faint dissolution rate of water-insoluble crystal. Abstract in 14th International Conference on Crystal Growth and 12th International Conference on vapor growth and epitaxy, ICCG14 Grenoble, France.
Onuma, K., Tsukamoto, K., and Sunagawa, I. (1989) Measurements of surface supersaturations around a growing K-alum crystal in aqueous solution. Journal of Crystal Growth, 98, 377–383.
Pina, C.M., Becker, U., Risthaus, P., Bosbach, D., and Putnis, A. (1998) Molecular-scale mechanisms of crystal growth in barite. Nature 395, 483–486.
Shiraki, R., Rock, P., and Casey, W.H. (2000) Dissolution kinetics of calcite in 0.1 *M* NaCl solution at room temperature: An atomic force microscopic (AFM) study. Aquatic Geochemistry, 6, 87–108.
Sorai, M., Ohsumi, T., and Ishikawa, M. (2002) AFM measurements of feldspar dissolution rates under supercritical CO_2-water-mineral system. Abstract in 2002 Joint Meeting for Earth and Planetary Science, J056-010.
Stillings, L.L. and Brantley S.L. (1995) Feldspar dissolution at 25 °C and pH 3: Reaction stoichiometry and the effect of cations. Geochimica et Cosmochimica Acta, 59, 1483–1496.
Stillings, L.L., Brantley, S.L., and Machesky, M.L. (1995) Proton adsorption at an adularia feldspar surface. Geochimica et Cosmochimica Acta, 59, 1473–1482.
Taylor, A., Blum, J.D., and Lasaga, A.C. (2000) The dependence of labradorite dissolution and Sr isotope release rates on solution saturation state. Geochimica et Cosmochimica Acta, 64, 2389–2400.
Tsukamoto, K. and van der Hoek, B. (1982) On the movement of mono-molecular steps on LPE grown garnets. Journal of Crystal Growth, 57, 131–140.
Tsukamoto, K., Onuma, K., and MacInnis, I. (1992) Application of real time phase shift interferometry to the slightly dissolved crystals in water. Proceedings of the Sixth Topical Meeting on Crystal Growth Mechanism, 227–231.

Manuscript received November 13, 2005
Manuscript accepted October 11, 2006
Manuscript handled by Andreas Luttge